Faculty Scholarship

2011

Unveiling Extragalactic Star Formation Using Radio Recombination Lines: An Expanded Very Large Array Pilot Study With Ngc 253

Amanda A. Kepley

Laura Chomiuk

Kelsey E. Johnson

W. M. Goss

Dana S. Balser

See next page for additional authors

Follow this and additional works at: https://researchrepository.wvu.edu/faculty_publications

Authors

Amanda A. Kepley, Laura Chomiuk, Kelsey E. Johnson, W. M. Goss, Dana S. Balser, and D. J. Pisano

UNVEILING EXTRAGALACTIC STAR FORMATION USING RADIO RECOMBINATION LINES: AN EXPANDED VERY LARGE ARRAY PILOT STUDY WITH NGC 253

Amanda A. Kepley[1,6], Laura Chomiuk[2,3,7], Kelsey E. Johnson[1,8], W. M. Goss[4], Dana S. Balser[2], and D. J. Pisano[5,8]

[1] Department of Astronomy, University of Virginia, P.O. Box 400325, Charlottesville, VA 22904-4325, USA; kepley@virginia.edu, kej7a@virginia.edu
[2] National Radio Astronomy Observatory, 520 Edgemont Road, Charlottesville, VA 22903-2475, USA; lchomiuk@cfa.harvard.edu, dbalser@nrao.edu
[3] Harvard-Smithsonian Center for Astrophysics, 60 Garden Street, Cambridge, MA 02138, USA
[4] National Radio Astronomy Observatory, Pete V. Domenici Science Operations Center, P.O. Box 0,
1003 Lopezville Road, Socorro, NM 87801-0387, USA; mgoss@nrao.edu
[5] Department of Physics, West Virginia University, 244 Hodges Hall, P.O. Box 6315, Morgantown, WV 26506, USA; DJPisano@mail.wvu.edu

ABSTRACT

Radio recombination lines (RRLs) are powerful, extinction-free diagnostics of the ionized gas in young, star-forming regions. Unfortunately, these lines are difficult to detect in external galaxies. We present the results of Expanded Very Large Array (EVLA) observations of the RRL and radio continuum emission at 33 GHz from NGC 253, a nearby nuclear starburst galaxy. We detect the previously unobserved H58α and H59α RRLs and make simultaneous sensitive measurements of the continuum. We measure integrated line fluxes of 44.3 ± 0.7 W m^{-2} and 39.9 ± 0.8 W m^{-2} for the H58α and H59α lines, respectively. The thermal gas in NGC 253 is kinematically complex with multiple velocity components. We constrain the density of the thermal gas to $(1.4–4) \times 10^4$ cm^{-3} and estimate an ionizing photon flux of 1×10^{53} s^{-1}. We use the RRL kinematics and the derived ionizing photon flux to show that the nuclear region of NGC 253 is not gravitationally bound, which is consistent with the outflow of gas inferred from the X-ray and Hα measurements. The line profiles, fluxes, and kinematics of the H58α and H59α lines agree with those of RRLs at different frequencies confirming the accuracy of the previous, more difficult, high-frequency observations. We find that the EVLA is an order of magnitude more efficient for extragalactic RRL observations than the Very Large Array. These observations demonstrate both the power of the EVLA and the future potential of extragalactic RRL studies with the EVLA.

Key words: galaxies: individual (NGC 253) – galaxies: ISM – galaxies: star formation – radio continuum: galaxies – radio lines: galaxies

1. INTRODUCTION

How stars form is one of the most important physical questions in astrophysics today. While we have viable theories that explain how star formation occurs in the Milky Way (Zinnecker & Yorke 2007; McKee & Ostriker 2007), we do not yet understand how stars form in galaxies with different conditions than those in the Milky Way. A key piece of the puzzle is quantitative information about the physical conditions in the interstellar medium (ISM) in extragalactic star-forming regions with a wide range of metallicities, total masses, and star formation rates. Studies of young star-forming regions still embedded in their natal clouds of dust and dense gas are particularly important; these embedded regions give us crucial information about the ISM before the newly formed stars have destroyed their birth environments and thus tell us about the conditions in which stars form. However, these regions are poorly understood because they are heavily obscured in the optical and near-infrared ($A_V \gtrsim 10$), which limits the utility of "standard" optical/IR nebular diagnostic lines.

Radio recombination lines (RRLs) are powerful tracers of the physical properties of obscured thermal gas. These lines occur when electrons make transitions between high levels ($n \gtrsim 40$) of an excited atom (Roelfsema & Goss 1992; Gordon & Sorochenko 2009). For typical extragalactic spatial resolutions, RRLs act like density filters with higher frequency lines tracing

higher density gas (Zhao et al. 1997). Observations of RRLs at multiple, widely spaced frequencies constrain the density and filling factor of the thermal gas in a star-forming region without being affected by the significant extinction from the dust and gas within the star-forming region. RRLs also provide kinematic information about the thermal gas and estimates of the ionizing photon flux, the star formation rate, and the star formation efficiency. Unfortunately, the use of RRLs outside the Milky Way system has been limited to a dozen bright, nearby galaxies because these lines are faint (a few percent above the continuum) and have large velocity widths ($\gtrsim 100$ km s^{-1}). Moreover, the higher frequency RRLs, which trace the higher density thermal gas and thus younger star-forming regions, have been particularly challenging to observe because the bandwidths needed to observe these lines were larger than the maximum available bandwidth of the previous generation of instrumentation.

Work by Anantharamaiah and collaborators established the Very Large Array (VLA) as a powerful instrument for extragalactic RRL observations (e.g., Anantharamaiah et al. 1993; Zhao et al. 1996; Anantharamaiah & Goss 1996; Zhao et al. 1997; Phookun et al. 1998; Anantharamaiah et al. 2000; Das et al. 2001; Mohan et al. 2001, 2002; Roy et al. 2005; Mohan et al. 2005; Roy et al. 2008).[9] Most of these observations were at frequencies $\lesssim 8.3$ GHz; this was the highest frequency for which the VLA correlator had a large enough velocity coverage to observe the entire line using a single correlator tuning. Observations of RRLs at higher frequencies (43 GHz)

---

[9] Roy et al. (2005, 2008) also include data from the Australia Telescope Compact Array.

by Rodríguez-Rico and collaborators required combining four correlator tunings in post-processing for the necessary velocity coverage (Rodríguez-Rico et al. 2004, 2005, 2006, 2007a, 2007b). While those observations provided vital information on the high-density gas in several systems, they may introduce systematic uncertainties in the line profile and in the continuum subtraction, particularly for very broad lines.

The bandwidth of the National Radio Astronomy Observatory (NRAO) Expanded Very Large Array (EVLA; Perley et al. 2011)[10] WIDAR correlator and the improved sensitivity and additional frequency coverage of the EVLA receivers are opening new frontiers in RRL studies. These improvements will make observations of these lines significantly more efficient than with the VLA enabling us to broaden the sample of galaxies with RRL measurements. We present observations taken as part of the EVLA Resident Shared Risk Observing (RSRO) program AK726 to test the RRL capabilities of the EVLA. The electronics of the EVLA are completely new, so the performance of the EVLA for detecting these lines cannot be directly extrapolated from the very successful attempts using the VLA.

For our pilot study, we chose NGC 253, a nearby galaxy with a nuclear starburst (Ulvestad & Antonucci 1997; Johnson et al. 2001; Fernández-Ontiveros et al. 2009). This galaxy is an ideal source to test the RRL capabilities of the EVLA because of its strong, well-studied RRL emission; it has measurements of 11 different RRLs from H166α to H40α (Seaquist & Bell 1977; Mebold et al. 1980; Anantharamaiah & Goss 1990, 1996; Puxley et al. 1997; Mohan et al. 2002, 2005; Rodríguez-Rico et al. 2006). We present observations of two, previously undetected RRLs (H58α and H59α). We demonstrate that the EVLA produces results comparable to previous VLA observations in an eighth of the time and allows simultaneous observations of multiple RRLs. With the bandwidth of the EVLA WIDAR correlator, we are able to more accurately derive the line profile and make excellent, simultaneous measurements of the continuum. We use the H58α and H59α lines to constrain the density of the thermal gas in NGC 253, estimate the ionizing photon flux, and explore the kinematics of the thermal gas in the nuclear region.

We assume that a distance to NGC 253 is 3.4 Mpc (1″ is 16 pc), which is the mean of the distances determined from three different fields using the tip of the red giant branch method (Dalcanton et al. 2009).

2. DATA REDUCTION

The data were taken with the EVLA in DnC configuration on 2010 September 22, 25–30. The angular resolution was approximately 1″8 with a field of view of 1′4. The resolution corresponds to a physical resolution of 30 pc, which is five to ten times the size of a typical massive star cluster. While these observations cannot resolve individual clusters, they are also unlikely to resolve out diffuse emission associated with the clusters.

We observed H58α (32.85220 GHz) and H59α (31.22332 GHz), which were previously undetected in NGC 253. We configured the correlator to provide two basebands, each containing eight adjacent 128 MHz wide sub-bands with 128 channels and dual polarization. We tuned the basebands to the sky frequencies corresponding to H58α and H59α

for NGC 253. The sensitivity at the edges of the sub-bands decreases, which increases the noise in this region of the spectrum by a factor of $\sim$1.4. The placement of the line peak at the edge of a sub-band results in the noise being higher in the region with the line peak. However, this placement allows very accurate measurements of the flux in the line wings.

We used J0137+3309 (3C48) and J0542+4951 (3C147) as absolute flux density calibrators, J0319+4130 as the bandpass calibrator, and J0137−2430 as the complex gain calibrator. The total on-source time was 57 minutes.

We used CASA[11] to calibrate the data using the standard EVLA high-frequency calibration method[12] with three modifications. First, since at the time these data were calibrated there were no Ka-band flux density calibrator models, we used the K-band flux density calibrator models. The next two modifications were used to ensure that each individual sub-band was on the same flux density scale. The average opacity value for the central two spectral windows was used as the opacity value for all spectral windows in a baseband. Since the opacity values typically vary by only 2%–3% across the entire baseband, this does not introduce any significant systematic effects. Finally, since the flux density derived for the complex gain calibrator was the same (within the errors) for each sub-band in one baseband, we set the flux density of the complex gain calibrator for each sub-band to be the average of the flux densities determined for the complex gain calibrator.

We self-calibrated using the continuum emission deriving one solution for each baseband. We continuum subtracted the data in $u - v$ space and combined the line data (shifting to the same reference frequency) and the continuum data. Table 1 lists the image properties.

3. RESULTS

Accurate measurements of both the RRL and continuum emission are necessary to model the RRL emission. Previous RRL observations sacrificed continuum sensitivity to detect and spectrally resolve the RRL. The bandwidth of the EVLA allows us, for the first time, to make sensitive, simultaneous measurements of both the RRL and continuum emission. Figure 1 shows the 33 GHz continuum and integrated H58α line flux density for NGC 253 overlaid on a *Hubble Space Telescope* (*HST*) image of the optical and IR emission. We do not show the 32 GHz or the H59α data since they are very similar. The strongest RRL emission is coincident with the peak of the radio continuum emission. There is another extended region of RRL emission toward the southwestern (SW) portion of the disk. Following Rodríguez-Rico et al. (2006), we refer to these regions as the northeastern (NE) and SW regions. We measured the flux in the NE region using a rectangle with a bottom left corner of (00^{h}47^{m}33^s.3, −25°17′19) and a top right corner of (00^{h}47^{m}33^s.0, −25°17′15) and the SW region using a rectangle with a bottom left corner of (00^{h}47^{m}33^s.1, −25°17′23) and a top right corner of (00^{h}47^{m}32^s.8, −25°17′19).

The extinction in this region is extremely high. In the *HST* image, blue (*B* band) represents unobscured young star formation, while the red (Paschen α) traces obscured recent star formation. The RRL emission is coincident with the highly extincted recent star formation south of the dust lane. The higher resolution of the *HST* data allows us to distinguish many of the individual star formation regions that are not resolved

---

[11] http://casa.nrao.edu
[12] http://casaguides.nrao.edu
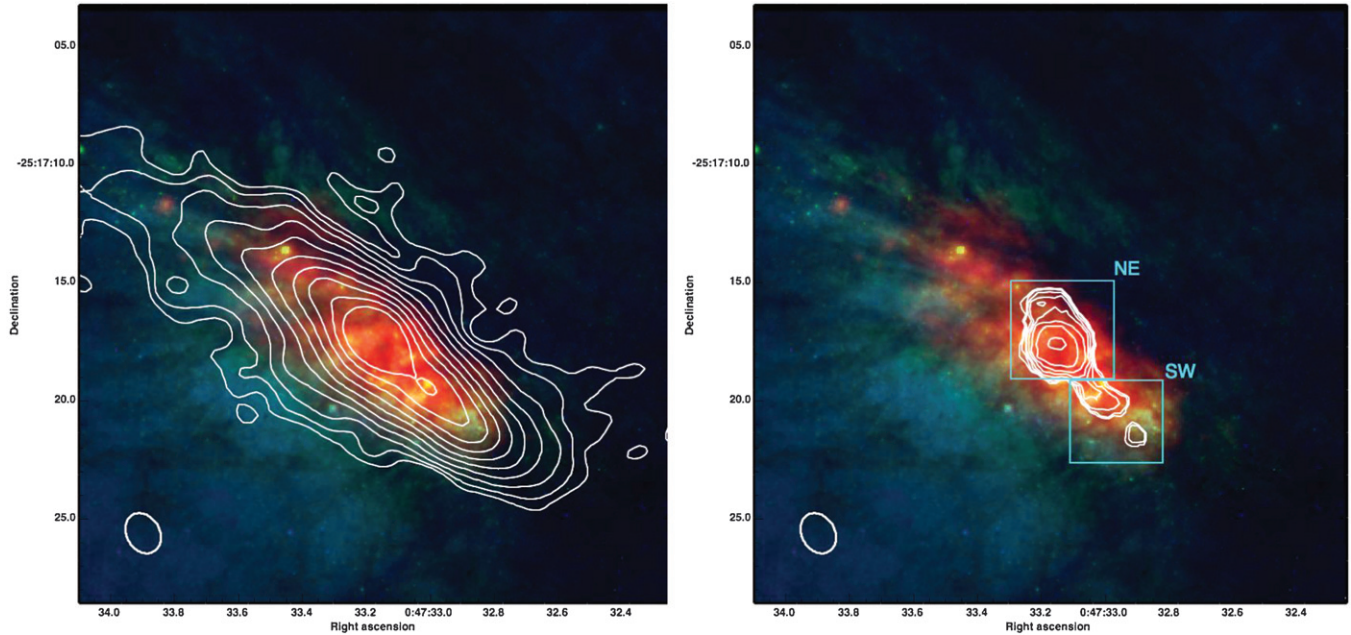
Figure 1. *HST* ACS (F475W and F814W) and NICMOS (F187N) images of NGC 253. The F187N filter (Paschen α) is red, the F814W filter (*I* band) is green, and the F475W filter (*B* band) is blue. Left: 33 GHz continuum contours from 5σ to 500σ on a logarithmic scale ($1\sigma = 0.09$ mJy beam^{-1}). Right: integrated H58α emission contours on a logarithmic scale between 5% and 90% of the peak flux of 1.15 Jy beam^{-1} km s^{-1}. The distribution of the 32 GHz continuum and H59α line emission is identical. The beam ($\sim 1\rlap{.}''8$) is shown in the lower left-hand corner of each panel.

Table 1
Image Properties

Line/IF	Frequency (GHz)	Type	Robust	Beam (″)	P.A. (°)	Noise (mJy beam^{-1})	Velocity Resolution (km s^{-1})	Bandwidth (MHz)
H58α	32.85220	Line	0	1.82×1.46	49.1	0.75	18.3	$\cdots$
H59α	31.22331	Line	0	1.80×1.62	60.3	1.3	19.2	$\cdots$
IF1	33.0	Continuum	0	1.75×1.38	58.5	0.09	$\cdots$	768
IF2	32.0	Continuum	0	1.85×1.40	64.8	0.16	$\cdots$	768

in the RRL observations. Even at the larger spatial resolution of the EVLA data, we can distinguish two separate, obscured star-forming regions associated with primary and secondary radio continuum and RRL peaks.

The distribution of the H58α line and 33 GHz continuum emission are similar to the distribution of the H53α line and 43 GHz continuum determined by Rodríguez-Rico et al. (2006). Both data sets have similar noise levels. The observing times required to reach these sensitivities, however, are drastically different. The on-source observing time for the data presented in Rodríguez-Rico et al. (2006) was 8 hr, while the H58α data was obtained in 57 minutes. The observations presented in Rodríguez-Rico et al. (2006) only measured one line and a small amount of continuum, while we measured two lines as well as obtained excellent continuum data at both line frequencies. This comparison shows that the EVLA is at least an order of magnitude more efficient than the VLA for extragalactic RRL observations. The 8 GHz bandwidth of the full correlator will deliver even higher observing efficiencies by providing simultaneous observations of at least four RRLs at these frequencies.

Figure 2 shows channel maps for the H58α emission. The NE and SW regions have different kinematics. The NE region covers a wide range of velocities from ~ 0 km s^{-1} to 360 km s^{-1}, while the SW region covers a much narrower range in velocities (190 km s^{-1} to 300 km s^{-1}). The central velocities of

the NE and SW region are offset by approximately 60 km s^{-1}. Anantharamaiah & Goss (1996) attribute the complex H92α velocity field to either a tumbling bar potential, the merger or accretion of another galaxy, or a warp in the disk in the nuclear region. Rodríguez-Rico et al. (2006) suggest that the RRL velocity structure could also be the result of an outflow driven by the nuclear starburst. There is additional X-ray and Hα evidence (Strickland et al. 2000; Westmoquette et al. 2011) supporting a nuclear outflow.

Figure 3 shows the spectrum for the entire line-emitting region and for the NE and SW regions. As expected from the models of these lines, the higher frequency (H58α) line has a higher peak flux density than the lower frequency line (H59α). The H58α and H59α line profiles for the entire RRL region are similar to the line profiles reported by Rodríguez-Rico et al. (2006) and show the presence of several kinematic components discussed in detail by Mohan et al. (2005). We averaged every three channels in the H58α cube together to compare the peak of the H58α line profile to the peak of the H53α line profile from Rodríguez-Rico et al. (2006). The line profiles agree well. The H53α peak line flux density is larger than the H58α peak line flux density, again in agreement with phenomenological expectations.

We fit Gaussians to the H58α and H59α line profiles. While Gaussians are not the best fit for the data because of the multiple velocity components, these fits allow us to directly compare our results to the fits for other RRLs in the literature. Table 2
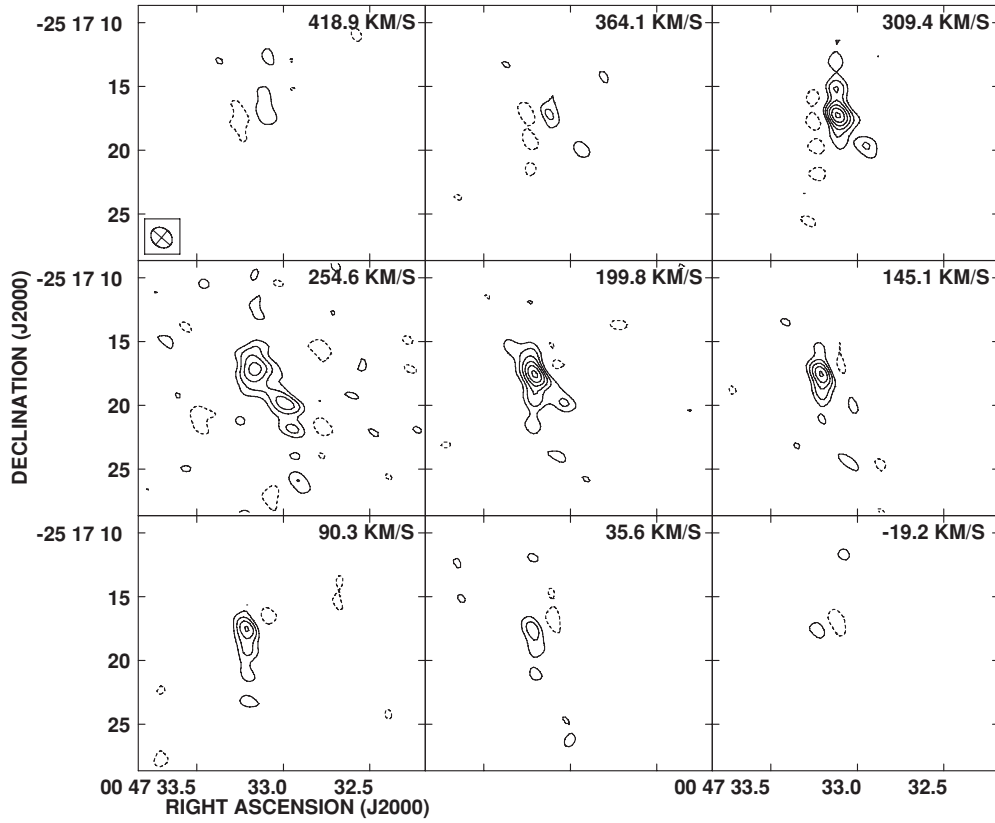
Figure 2. Channel images for H58α emission. For this figure, we have averaged every three channels together. The contours are -3σ, 3σ, 5σ, 7σ, 9σ, etc. ($1\sigma = 0.43$ mJy beam^{-1}). The upper right-hand corner of each panel gives the heliocentric velocity (optical definition). The lower left-hand corner of the first panel shows the beam ($\sim 1\farcs8$).

Table 2
RRL Parameters

Region	Line	$\nu_{\rm rest}$ (GHz)	S_c (mJy)	S_L (mJy)	$\Delta V_{\rm FWHM}$ (km s^{-1})	$V_{\rm hel}$ (km s^{-1})	$S_L \Delta V_{\rm FWHM}$ (10^{-22} W m^{-2})	Ref.
Total	H58α	32.85220	314.27 ± 0.05	17.5 ± 0.3	158 ± 3	231 ± 1	44.3 ± 0.7	2
Total	H59α	31.22331	332.5 ± 0.1	16.3 ± 0.2	209 ± 3	222 ± 1	39.9 ± 0.8	2
NE	H58α	32.85220	241.63 ± 0.04	11.4 ± 0.2	169 ± 3	228 ± 1	28.6 ± 0.5	2
NE	H59α	31.22331	260.06 ± 0.07	11.8 ± 0.2	200 ± 3	206 ± 1	26.8 ± 0.5	2
SW	H58α	32.85220	83.19 ± 0.03	6.1 ± 0.2	159 ± 5	231 ± 2	15.6 ± 0.4	2
SW	H59α	31.22331	84.77 ± 0.05	4.6 ± 0.1	145 ± 7	256 ± 3	12.8 ± 0.4	2
Archival Data								
Total	H53α	43.3094	360 ± 20	21 ± 2	230 ± 20	210 ± 10	69 ± 9	1
Total	H92α	8.3094	605 ± 10	9.0 ± 0.5	190 ± 10	206 ± 4	4.7 ± 0.5	1
NE	H53α	43.3094	134 ± 5	9.0 ± 0.5	200 ± 10	220 ± 5	25 ± 1	1
NE	H92α	8.3094	278 ± 10	4.5 ± 0.1	190 ± 5	200 ± 2	2.4 ± 0.2	1
SW	H53α	43.3094	24 ± 2	2.8 ± 0.3	130 ± 20	215 ± 10	4 ± 1	1
SW	H92α	8.3094	40 ± 4	0.7 ± 0.1	160 ± 15	220 ± 10	0.3 ± 0.03	1

References. (1) Rodríguez-Rico et al. 2006; (2) This work.

gives the parameters for the fit to the lines as well as the fits presented in Rodríguez-Rico et al. (2006). The H58α and H59α measurements in this Letter agree with the measurements of the line flux from the literature. Differences between the flux measurements for each region in the current and archival data can be attributed to differences in the regions selected. The differing velocity widths of the H58α and H59α are due to systematic uncertainties in the Gaussian fits because of multiple velocity components and the different sensitivities of the two

images. The signal to noise of the H58α data is higher than that for the H59α data because the H59α line is fainter than the H58α line and the noise in the H59α cube is slightly higher.

Extragalactic RRL emission is modeled as a collection of H II regions, each with an identical electron density (n_e), size (l), and temperature (T), immersed in a region of diffuse radio continuum emission (Puxley et al. 1991; Anantharamaiah et al. 1993, 2000). We use the method of Zhao et al. (1997) to estimate the range of densities consistent with the H58α line data to

4
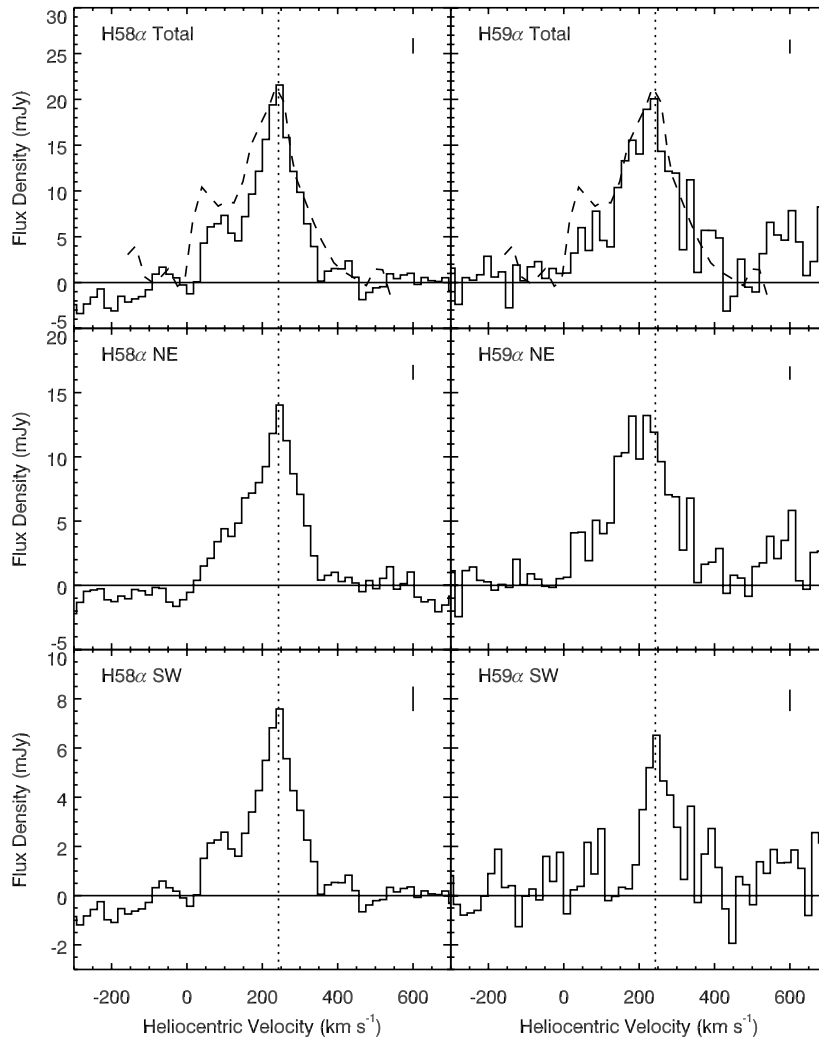
Figure 3. H58α (left panels) and H59α (right panels) emission for the entire RRL region (top row), the NE region (middle row), and the SW region (bottom row). The positions of each region are indicated in Figure 1. The horizontal line indicates a flux density of 0 mJy. The dotted vertical line indicates the boundary between two sub-bands. The line in the upper right-hand corner of each panel is the 3σ per channel error for each region. The dashed line in the top row is the H53α line profile from Rodríguez-Rico et al. (2006). The velocities are heliocentric (optical definition).

compare with those derived in the literature using other RRLs. Assuming a typical non-thermal spectral index (−0.7) and a temperature of 10^4 K, H58α line flux and continuum flux density are consistent with electron densities of $(1.4–4) \times 10^4$ cm^{-3}. This corresponds to an ionizing photon flux of 10×10^{52} s^{-1}. Using Equation (1) in Anantharamaiah et al. (2000), we obtain star formation rates averaged over the lifetime of OB stars of $2\,M_\odot$ yr^{-1} in the RRL emission region. The electron density, ionizing photon fluxes, and star formation rate estimates derived from the H58α line agree with those in the literature (Mohan et al. 2005; Rodríguez-Rico et al. 2006). Our ionizing photon flux is slightly higher, 10×10^{52} s^{-1}, than the $(3–6) \times 10^{52}$ s^{-1} ionizing photon flux derived by Mohan et al. (2005).

We use the derived ionizing photon flux and the measured line widths to estimate whether the nucleus of NGC 253 is gravitationally bound (e.g., Turner et al. 2003). We estimate the mass of the cluster from the number of ionizing photons using Leitherer et al. (1999). We assume that the cluster was formed in an instantaneous burst, is 3 Myr old (Fernández-Ontiveros et al. 2009), and has a Salpeter initial mass function with an upper mass limit of $100\,M_\odot$, which gives a cluster mass of $4.0 \times 10^6\,M_\odot$. The mass of the ionized gas derived by Rodríguez-

Rico et al. (2006) is negligible compared to the cluster mass. The line-emitting region is 53 pc by 135 pc. The escape velocity for the nucleus is then between 17 km s^{-1} and 26 km s^{-1}. This width is much smaller than the velocity width of the RRL emission. We assume that the RRL line widths are dominated by the motion of the gas since they are much larger than the intrinsic width of an RRL from a single H II region ($\sim$20 km s^{-1}). The escape velocity is still much smaller than the RRL velocity width if we consider only the NE region. There we derive an ionizing photon flux of 9.3×10^{52} s^{-1}, a cluster mass of $3.97 \times 10^6\,M_\odot$, and an escape velocity of 25 km s^{-1}. These calculations show that the central region of NGC 253 is most likely not gravitationally bound, supporting the hypothesis that there is an outflow of gas from the nucleus of this galaxy.

Although RRLs provide an extinction-free tracer of the gas ionized by the cluster, the use of RRL data may underestimate the number of ionizing photons if the photons are absorbed by dust rather than ionized hydrogen. Therefore, the mass of the cluster is a lower limit. To obtain an escape speed comparable to the RRL velocity width, the number of ionizing photons would have to be underestimated by a factor of 45.

4. CONCLUSIONS

We have presented observations of the H58α and H59α RRLs and the continuum emission at 32 and 33 GHz from the nucleus of NGC 253. We measure integrated line fluxes of 44.3 ± 0.7 and 39.9 ± 0.8 W m^{-2} for the H58α and H59α lines, respectively. We constrain the thermal gas density to $(1.4–4) \times 10^4$ cm^{-3}. We derive an ionizing photon flux of 10×10^{52} s^{-1}. These estimates of the density and ionizing photon flux are consistent with estimates from the literature (Mohan et al. 2002, 2005; Rodríguez-Rico et al. 2006).

The kinematics of the thermal gas in NGC 253 are complex. The NE region has a broader velocity width (170–200 km s^{-1}) than the SW region (145–159 km s^{-1}). From our estimate of the ionizing photon flux, we estimate a cluster mass for the nuclear region of NGC 253 of 4×10^6 $M_{\odot}$. The escape velocity for this mass is only 17 km s^{-1} to 26 km s^{-1}: much lower than the H58α and H59α velocity widths. Therefore, the nuclear region of NGC 253 is most likely not gravitationally bound. We suggest that an outflow of gas from the nuclear region is the most likely explanation for the thermal gas kinematics of NGC 253. The presence of this outflow has been inferred from X-ray (Strickland et al. 2000) and Hα (Westmoquette et al. 2011) observations.

In contrast to previous VLA high-frequency RRL observations, we were able to detect not one, but two RRLs, and make much more sensitive measurements of the continuum in an eighth of the time on source. Accurate measurements of both the RRL and continuum emission are necessary to model the RRL emission from these regions in detail. The EVLA is currently an order of magnitude more efficient for high-frequency RRL observations than the VLA. The EVLA observing efficiency will increase even further once the full 8 GHz bandwidth is available.

These observations demonstrate the potential of the EVLA to revolutionize extragalactic RRL observations. Future EVLA observations will be able to use RRLs to measure the properties of the thermal gas in a wider variety of galaxies. Ultimately, these observations will lead to a quantitative picture of how the properties of the ISM affect the resulting stellar populations.

Facility: EVLA

REFERENCES

Anantharamaiah, K. R., & Goss, W. M. 1990, in IAU Colloq. 125, Radio Recombination Lines: 25 Years of Investigation, ed. M. A. Gordon & R. L. Sorochenko (Astrophysics and Space Science Library, Vol. 163; Dordrecht: Kluwer), 267
Anantharamaiah, K. R., & Goss, W. M. 1996, ApJ, 466, L13
Anantharamaiah, K. R., Viallefond, F., Mohan, N. R., Goss, W. M., & Zhao, J. H. 2000, ApJ, 537, 613
Anantharamaiah, K. R., Zhao, J.-H., Goss, W. M., & Viallefond, F. 1993, ApJ, 419, 585
Dalcanton, J. J., Williams, B. F., Seth, A. C., et al. 2009, ApJS, 183, 67
Das, M., Anantharamaiah, K. R., & Yun, M. S. 2001, ApJ, 549, 896
Fernández-Ontiveros, J. A., Prieto, M. A., & Acosta-Pulido, J. A. 2009, MNRAS, 392, L16
Gordon, M. A., & Sorochenko, R. L. (ed.) 2009, Radio Recombination Lines (Astrophysics and Space Science Library, Vol. 282, Berlin: Springer)
Johnson, K. E., Kobulnicky, H. A., Massey, P., & Conti, P. S. 2001, ApJ, 559, 864
Leitherer, C., Schaerer, D., Goldader, J. D., et al. 1999, ApJS, 123, 3
McKee, C. F., & Ostriker, E. C. 2007, ARA&A, 45, 565
Mebold, U., Shaver, P. A., Bell, M. B., & Seaquist, E. R. 1980, A&A, 82, 272
Mohan, N. R., Anantharamaiah, K. R., & Goss, W. M. 2001, ApJ, 557, 659
Mohan, N. R., Anantharamaiah, K. R., & Goss, W. M. 2002, ApJ, 574, 701
Mohan, N. R., Goss, W. M., & Anantharamaiah, K. R. 2005, A&A, 432, 1
Perley, R. A., Chandler, C. J., Butler, B. J., & Wrobel, J. M. 2011, ApJ, 739, L1
Phookun, B., Anantharamaiah, K. R., & Goss, W. M. 1998, MNRAS, 295, 156
Puxley, P. J., Brand, P. W. J. L., Moore, T. J. T., Mountain, C. M., & Nakai, N. 1991, MNRAS, 248, 585
Puxley, P. J., Mountain, C. M., Brand, P. W. J. L., Moore, T. J. T., & Nakai, N. 1997, ApJ, 485, 143
Rodríguez-Rico, C. A., Goss, W. M., Turner, J. L., & Gómez, Y. 2007a, ApJ, 670, 295
Rodríguez-Rico, C. A., Goss, W. M., Viallefond, F., et al. 2005, ApJ, 633, 198
Rodríguez-Rico, C. A., Goss, W. M., Viallefond, F., et al. 2007b, ApJ, 668, 625
Rodríguez-Rico, C. A., Goss, W. M., Zhao, J.-H., Gómez, Y., & Anantharamaiah, K. R. 2006, ApJ, 644, 914
Rodríguez-Rico, C. A., Viallefond, F., Zhao, J.-H., Goss, W. M., & Anantharamaiah, K. R. 2004, ApJ, 616, 783
Roelfsema, P. R., & Goss, W. M. 1992, A&AR, 4, 161
Roy, A. L., Goss, W. M., & Anantharamaiah, K. R. 2008, A&A, 483, 79
Roy, A. L., Goss, W. M., Mohan, N. R., & Anantharamaiah, K. R. 2005, A&A, 435, 831
Seaquist, E. R., & Bell, M. B. 1977, A&A, 60, L1
Strickland, D. K., Heckman, T. M., Weaver, K. A., & Dahlem, M. 2000, AJ, 120, 2965
Turner, J. L., Beck, S. C., Crosthwaite, L. P., et al. 2003, Nature, 423, 621
Ulvestad, J. S., & Antonucci, R. R. J. 1997, ApJ, 488, 621
Westmoquette, M. S., Smith, L. J., & Gallagher, J. S., III 2011, arXiv:1103.1775
Zhao, J.-H., Anantharamaiah, K. R., Goss, W. M., & Viallefond, F. 1996, ApJ, 472, 54
Zhao, J.-H., Anantharamaiah, K. R., Goss, W. M., & Viallefond, F. 1997, ApJ, 482, 186
Zinnecker, H., & Yorke, H. W. 2007, ARA&A, 45, 481